Journal of Medicinal and Nanomaterials Chemistry 4 (2021) 282-294

SPC

Journal of Medicinal and Nanomaterials Chemistry

Journal homepage: https://jmnc.samipubco.com/

Original Research Article

Synthesis, structural evaluation of molybdenum oxide (MoO_3) nanoparticles and its application as CO_2 gas sensor

M.V. Manasa[a,b], G. Sarala Devi[a,b]*

[a] *Polymer and Functional Materials Division, CSIR-Indian Institute of Chemical Technology (CSIR-IICT), Habsiguda, Hyderabad -500007, India*

[b] *Academy of Scientific and Innovative Research (AcSIR), Ghaziabad – 201 002, India*

ARTICLE INFORMATION

Received: 29 June 2021
Received in revised: 4 August 2021
Accepted: 7 August 2021
Available online: 30 September 2021

DOI: 10.48309/JMNC.2021.4.5

KEYWORDS

MoO_3 Nanoparticles
Hydrothermal protocol
XRD
XPS
TEM

ABSTRACT

In the present study we report a simple eco-friendly hydrothermal protocol for the synthesis of molybdenum oxide (MoO_3) nanoparticles at various temperatures i.e., 80-200 °C at intervals of 20 °C designated as S1-S6 sequentially with time duration of 4 h for each batch. The synthesized samples were characterized by X-Ray Fluorescence (XRF), X-Ray Diffraction (XRD), Fourier Transform Infra-red (FTIR), UV- Visible Diffuse Reflectance (UV-Vis DRS), Laser Raman, Cyclic Voltammetry (CV), X-Ray Photoelectron Spectroscopy (XPS) and Transmission Electron Microscopy (TEM) to find out their elemental composition, structure, morphology and the optical band gap. The XRD analysis indicates well-crystallized orthorhombic structure with preferred orientation along (210) plane. The presence of O-Mo-O stretching vibration was observed by FTIR analysis The gas sensing studies were carried out to examine the material's Sensitivity over a temperature range of 50°C to 400°C for various gas concentrations i.e. 200-1000 ppm of CO_2 gas. The sensor had a Sensitivity of S=68.5% for S4 sample at an optimum temperature of 200 °C. The adsorption of desired gas on the material correlated well with the particle size of material at different temperature. The response and recovery times were 50 s and 40 s respectively.

Corresponding author, email: sarala@csiriict.in (S. Sarala Devi).
Tel.: 09703221678.

Graphical Abstract

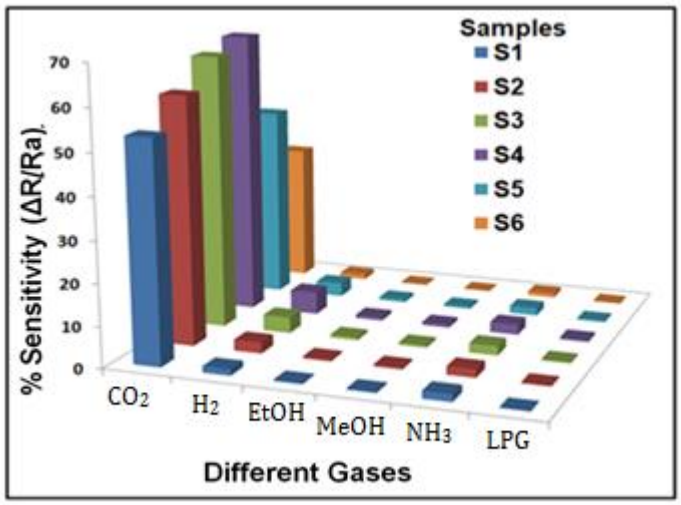

Introduction

Nano materials offer unique properties enabling the development and cost efficient production of components that operate faster with higher efficiency, less power consumption [1]. A variety of materials in their nano forms such as titanium oxide, zinc oxide, silica, carbon nanotubes, polymers, etc. are being used to make air clean, purify water and decontaminate soil [2–6]. The physical properties of nanomaterials differ from bulk materials and others of different dimensions such as nanoparticles, nano wires, nano plates, imprinted polymeric spheres, etc. [7, 8]. This uniqueness offers more opportunities to fine-tune the bandgap of materials. Further Nanomaterials exhibit quantization and electronic confinement effects, which can be applied in various fields of Science and Technology such as development of sensors for environmental and industrial monitoring, optoelectronics, biomedicine, catalysis, miniaturized devices, healthcare, genetics, diagnostics, drug discovery quality control, etc. [9, 10]. In this context, semiconducting oxides have come under intense scrutiny for the possibility of high conductivity, enhanced chemical stability, low toxicity, corrosion resistance and cost effectiveness [11–14].

Molybdenum trioxide (MoO_3), an n-type semiconducting metal oxide is one of the most important transition metal oxides as it is thermally stable having high melting point and high chemical stability [15–17]. Hence it has potential applications in various fields such as catalysis, lubricants, solar cells, lithium-ion batteries, display materials, etc. [18–24]. However, its properties depend significantly upon the adopted synthetic procedures and various experimental conditions such as reaction time, temperature, etc. [25–27].

There are various synthesis methods adopted such as Sol-Gel, Solution Combustion, Infrared Irradiation, Sputtering, Microwave, Hydrothermal, Electrochemical, Sono-chemical, etc. [28–30]. Amongst these, hydrothermal method has unique advantages in terms of high reactivity and easy control of interface reactions and enables to produce stable and condensed phases with low energy consumption and less environmental pollution

without emitting any harmful gases [31, 32]. Ganguly A. *et al*. reported the synthesis of MoO_3 nanoparticles of 100nm via citrate Sol-Gel method at 250 °C /1h followed by calcination at 500 °C. [33] The synthesis of MoO_3 nanoparticles via solution combustion method employing ammonium hepta molybdate (AHM) at 470 °C was reported by Nagabhushana G.P. *et al*. [34]. Microwave assisted synthesis of MoO_3 nanoparticles was reported by Arumugam M. *et al*. [35] involving high power of 70 Watts.

In the present study we adopted a simple, eco-friendly hydrothermal protocol for the synthesis of molybdenum oxide (MoO_3) nanoparticles at various reaction temperatures i.e., 80–200 °C at intervals of 20 °C designated as S1-S6 sequentially.

Experimental

Materials and Methods

Molybdenum oxide nanoparticles were synthesized by hydrothermal protocol. In a typical synthesis procedure,1M PEG was dissolved in 100 mL of D.I. water to which 2M Ammonium molybdate ($(NH_4)_6Mo_7O_{24}.4H_2O$) was added and stirred for 4 h. The solution was transferred into an autoclave and set at 150 °C and processed for 4 h. After completion of the reaction it was cooled, centrifuged at 4000 rpm and oven dried. The obtained sample was calcined at 400 °C for 2h to obtain MoO_3 nanoparticles. Similar experiments were carried out at different temperatures i.e., 80-200 °C at intervals of 20 °C designated as S1-S6.

Equipment used for characterization of MoO_3 Nanoparticles

X-Ray Fluorescence (XRF) was recorded on OCEAN PUMA 7600D spectrometer. X-Ray Diffraction data were recorded on the Siemens (D5000) diffractometer using CuKα radiation (λ=1.54A^o) in the range of 2θ=20^o-80^o. Fourier Transform Infrared Spectra (FTIR) were recorded on a Bruker DF6 model and UV-Vis DRS were recorded on Perkin Elmer U-2910 UV double beam spectroscopy. Raman Spectra were recorded on RUBY-D-RAMAN E7563-2009 model. Cyclic Voltametry (CV) results were recorded in Corrtest CS350 model measured in 0-3V voltage range. X-Ray Photoelectron Spectroscopic data were recorded on KRATOS-Axis supra model spectroscope and Transmission Electron Microscopy (TEM) images were recorded on TEM-TALOS L120C model. Surface area analysis was carried out on a BET Analyzer Quantachrome AS-3012 model.

Results and Discussion

X-Ray Fluorescence Spectroscopy (XRF)

The XRF for S1-S6 samples showed the presence of Mo and O signals in all the samples without any impurity. Here, a representation spectrum of MoO_3 nanoparticles for S4 sample is shown in Figure 1 which confirm the presence of Mo and O signals.

The XRD pattern of all MoO_3 samples (S1-S6) show similar (h k l) values i.e., (101), (400), (2 1 0), (1 1 1), (6 0 0), (1 0 2) & (0 2 0) planes at 23.31^o, 25.70^o, 27.33^o, 33.74^o, 38.98^o, 46.21^o and 49.26^o 2θ values respectively as shown in Figure 2 and are incoherence with the JCPDS data (no. 897112) with lattice constants a=13.85A^o, b=3.69A^o, c=3.96A^o and lattice angles α=β=γ=90^o. The average crystallite size (D) was calculated using the Scherer's formula given below.

$$D = \frac{K.\lambda}{\beta.Cos\theta} \quad (1)$$

Where K indicates the Scherrer's constant (0.9), λ is the wavelength of X-Ray (1.54A^o), β is full width half maximum of each peak in

respective XRD pattern and θ is the Bragg's angle of diffraction. The crystallite size of MoO_3 samples (S1-S6) were calculated as 83.47, 30.65, 18.74, 14.26, 89.95 and 102.59 nm respectively. It is observed that the crystallite size decreased till 150 °C and increased with further increase in the temperature, perhaps due to nucleation of MoO_3 particles which in-turn resulted in the larger crystallite size.

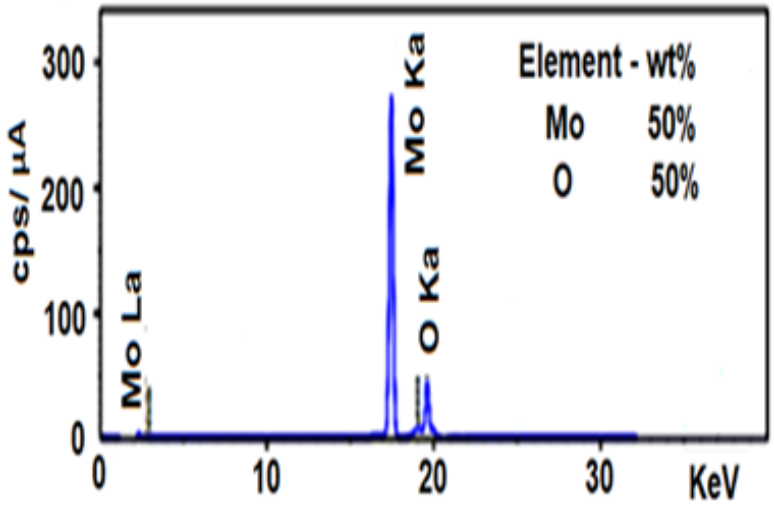

Figure 1. XRF spectrum of MoO_3 nanoparticles *X-Ray Diffraction (XRD) analysis*

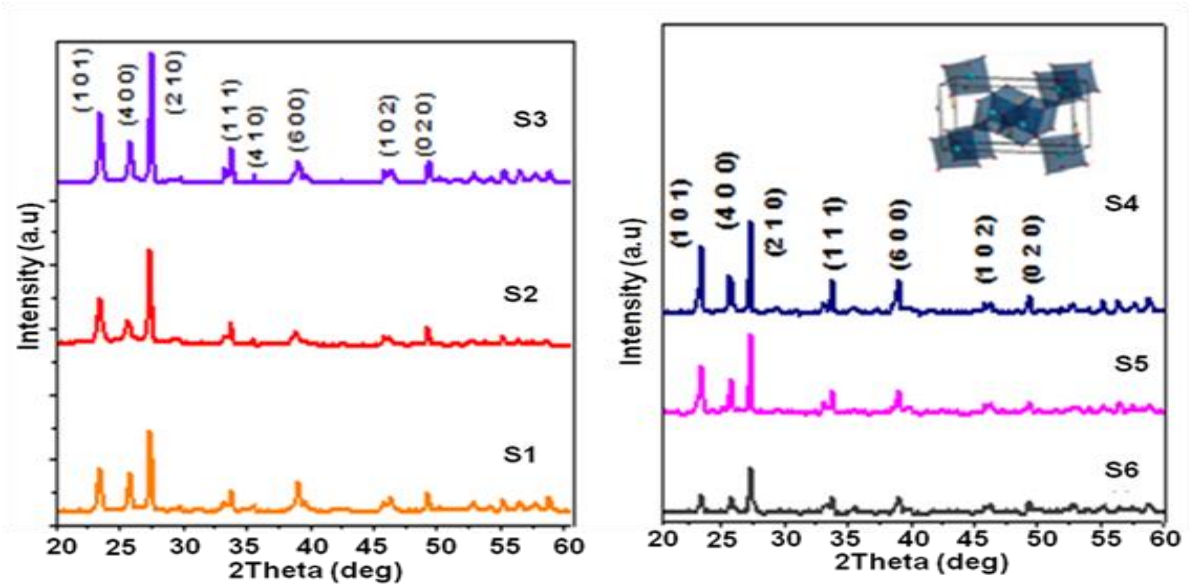

Figure 2. XRD pattern of MoO_3 nanoparticles samples S1-S6

Fourier Transform Infrared Spectroscopy (FT-IR)

The FT-IR spectra of MoO_3 nanoparticles viz., S1-S6, is depicted in Figure 3. Three peaks at 612.2 cm^{-1}, 875.4 cm^{-1} and 1001.8 cm^{-1} are characteristic of MoO_3. The peak at 1001.8 cm^{-1} is due to the terminal Mo–O bonding in the layered orthorhombic phase MoO_3. Absorption at 875.4 cm^{-1} is attributed to Mo–O–Mo vibrations of Mo^{6+}. And the peak at 612.28 cm^{-1}

is assigned to bending vibration of Mo–O–Mo entity.

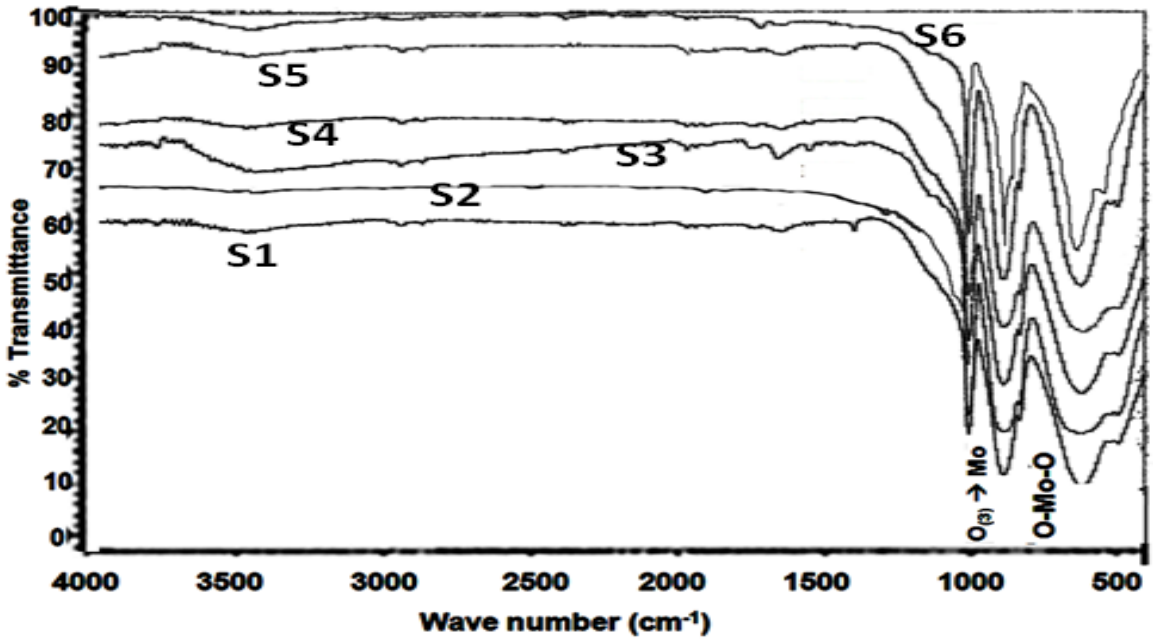

Figure 3. FT-IR spectra of MoO_3 nanoparticles synthesized hydrothermally, (S1) 80 °C (S2) 100 °C (S3) 120 °C (S4) 150 °C (S5) 170 °C (S6) 200 °C

UV-Visible Diffuse Reflectance spectroscopy (UV-DRS)

The UV-Vis diffuse reflectance spectroscopy is shown in the inset of Figure 4 and the bandgap calculated from respective Tauc plots obtained from UV-Vis DRS data for samples S1-S6 are 1.33 eV, 2.21 eV, 2.60 eV, 3.71 eV, 2.68 eV and 2.45 eV which are well in agreement with the reported semiconductor bandgap. It can be attributed to the intrinsic bandgap for absorption of MoO_3 nanoparticles. The bandgap (E_g) was estimated from Tauc plot, $(F(R)h\nu)^{1/2}$ versus the energy of photon ($h\nu$). Kubelka–Munk function F(R) was calculated using the following Eq. (2) by analyzing the UV-DRS results.

$$F(R) = \frac{(1-R)^2}{2R} \quad (2)$$

Where R is the reflectance (%) [35].

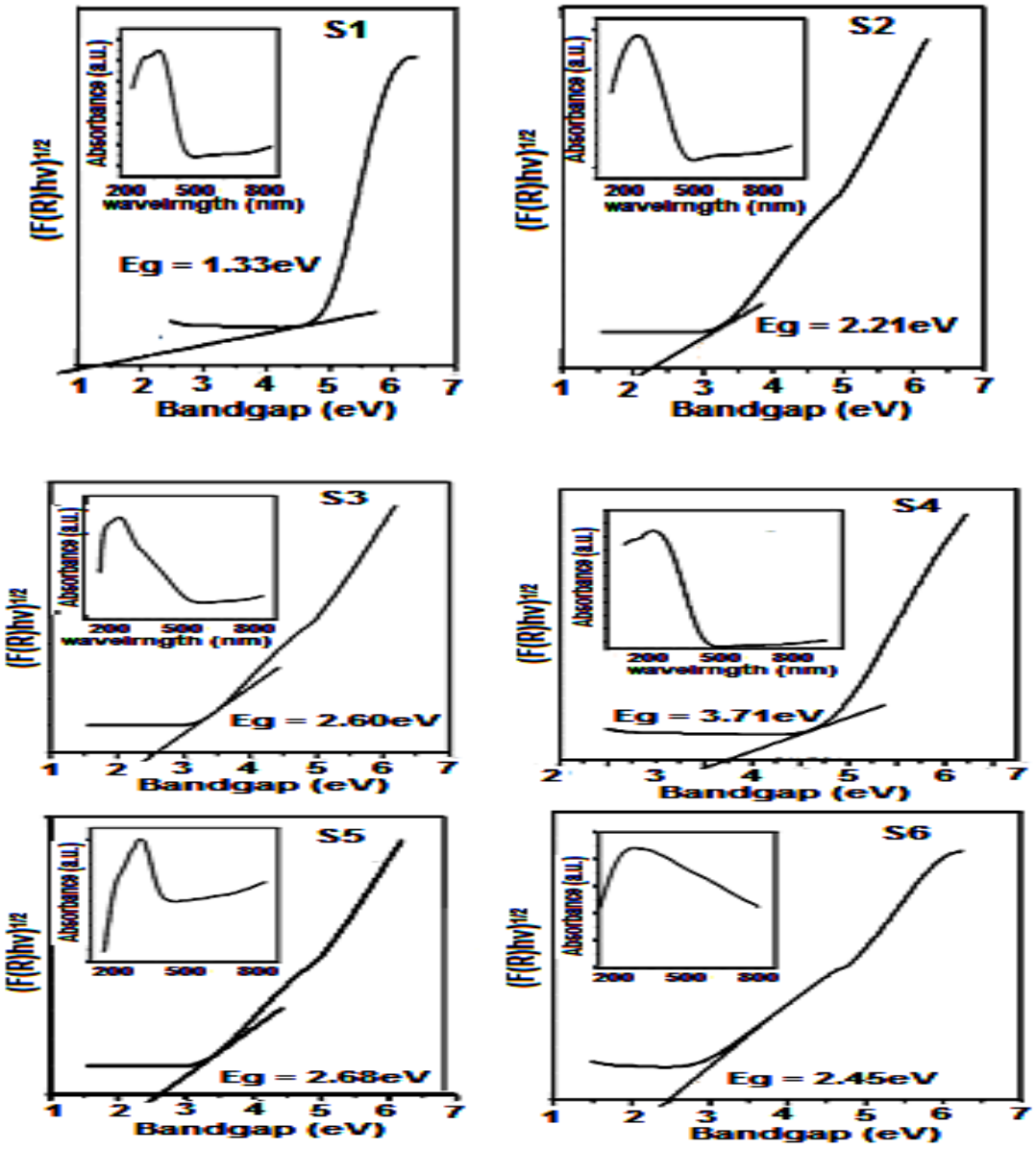

Figure 4. Diffuse Reflectance UV spectra of MoO_3 nanoparticles synthesized hydrothermally, (S1) 80 °C (S2) 100 °C (S3) 120 °C (S4) 150 °C (S5)170 °C and (S6) 200 °C

Raman Spectroscopy

The Raman spectra of samples S1-S6 at room temperature and the non-polarized Raman spectra measured in the quasi backscattering geometry in the region of the transverse optical (TO) phonons in the out planes of the sample surface is illustrated in Figure 5. The peaks observed in the range 748.3–812.8 cm^{-1} and 621.2–689.5 cm^{-1} are assigned to MoO_3 nanoparticles attributed to the second order Raman processes involving acoustic phonons this is comparable to the reported value.

Cyclic Voltammetry (CV)

The Current-Voltage (I-V) characteristics of MoO_3 samples (S1-S6) measured over a voltage

range of 0-3V is depicted in Figure 6. The maximum current for the samples are observed at 0.18 µA, 0.21 µA, 0.30 µA, 0.35 µA, 0.33 µA and 0.31 µA respectively. The sample S4 exhibits higher current which may be due to high electron discharge rates within the grain boundaries of the particles compared to other samples [36].

X-Ray Photoelectron spectroscopy (XPS)

Figure 7a depicts the survey scan of the synthesized MoO_3 nanoparticles where the peaks at 266eV and 285.93eV correspond to $Mo3d_{3/2}$ and $Mo3d_{5/2}$ orbits respectively and the peak observed at 431.64eV is assigned to O-1 s orbit which reveals the Mo–O bond formation in MoO_3 nanoparticles. In Figure 7b the Mo3d core level spectrum reveals the spin orbit splitting of $Mo3d_{3/2}$ ground state to be 265.19 eV while $Mo3d_{5/2}$ excited state is observed at 277.48 eV which is attributed to Mo^{+6}. A broadband observed at 533.05eV (Figure 7c) corresponds to O-1 s core level.

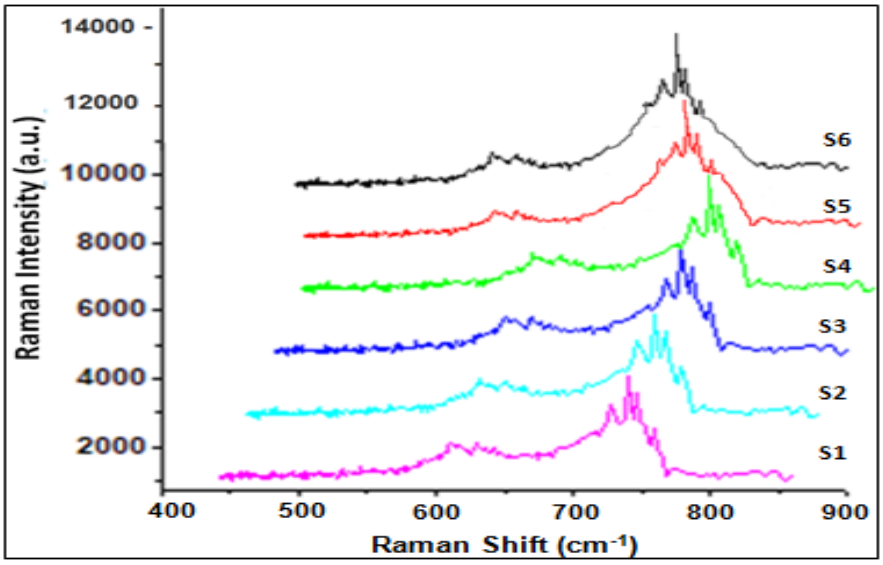

Figure 5. Raman spectra of samples synthesized hydrothermally, (S1) 80 °C (S2) 100 °C (S3) 120 °C (S4) 150 °C (S5) 170 °C and (S6) 200 °C

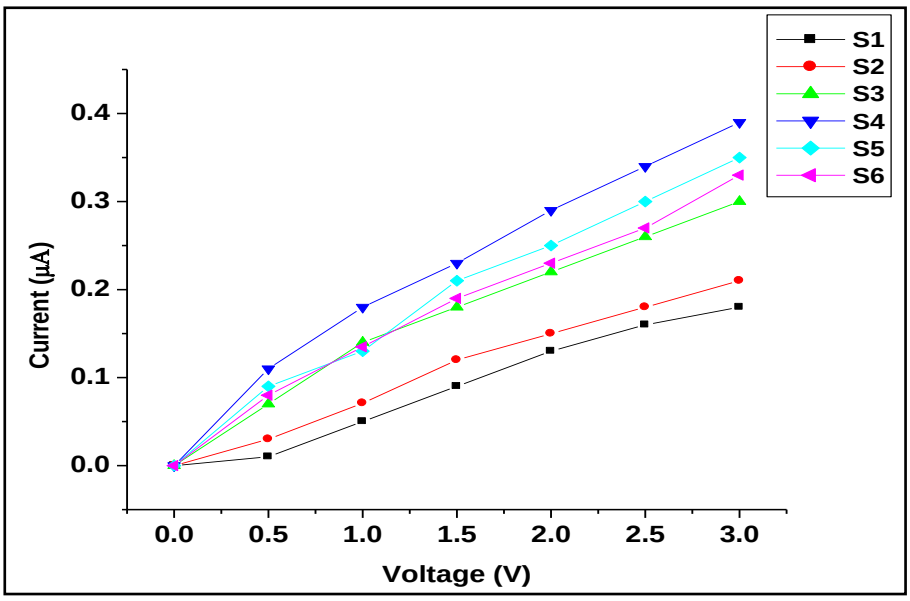

Figure 6. I-V Characteristics of MoO_3 samples synthesized hydrothermally, (S1) 80 °C (S2) 100 °C (S3) 120 °C (S4) 150 °C (S5) 170 °C and (S6) 200 °C

Transmission Electron Microscopy (TEM)

The TEM micrographs of the synthesized MoO_3 nanoparticles i.e., samples S1-S6 are shown in Figure 8**a–f** which reveals the orthorhombic structure of MoO_3 nanoparticles. The least particle size is observed as ~22 nm for S4 Sample, which is in agreement with the crystallite size calculated from XRD analysis. The characterization results of all these samples are given in Table 1.

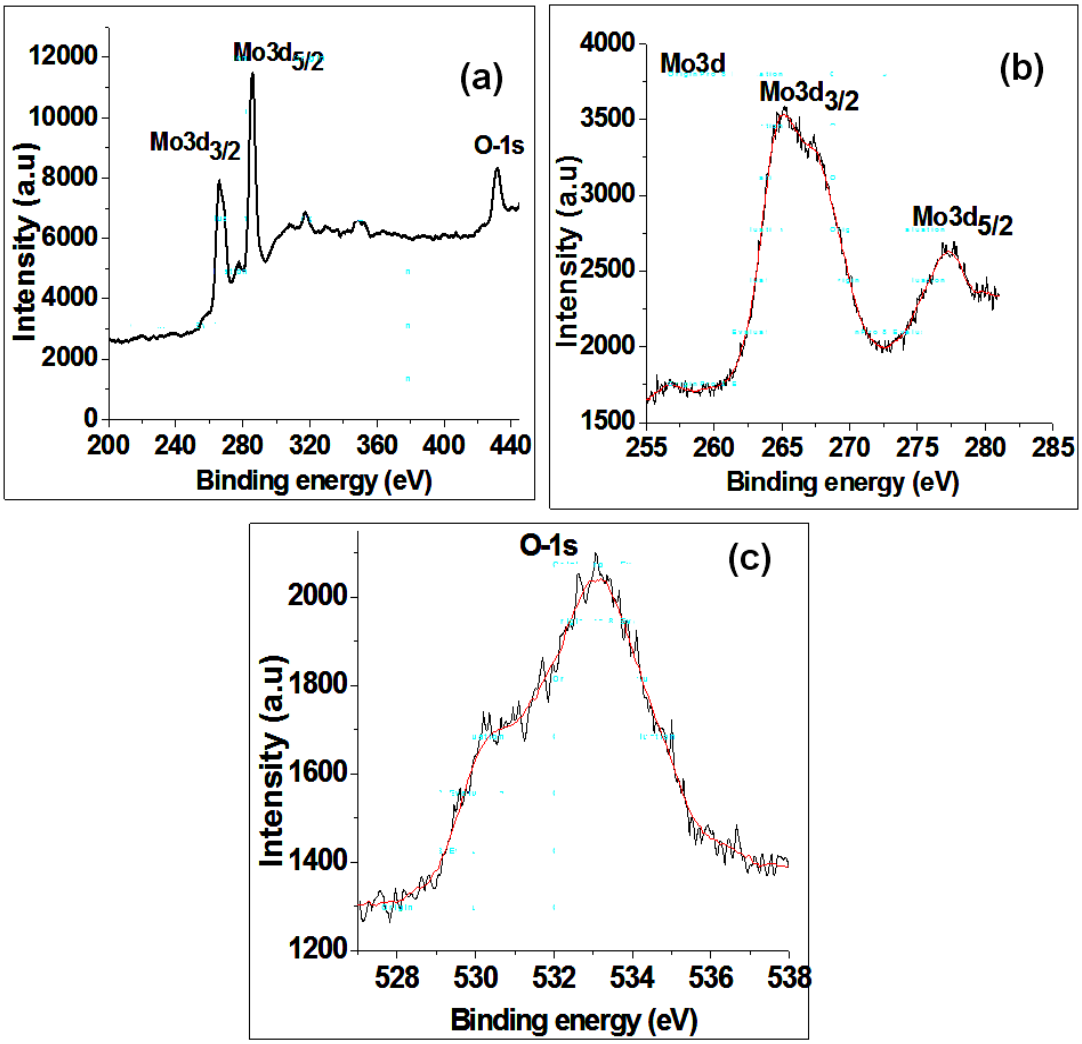

Figure 7. XPS spectrum of a) MoO_3 nanoparticles, b) Mo3d and c) O1s core level

Table 1. Summary of characterization results of Nano MoO_3 samples S1-S6

Sample	[a] Surface Area (m^2/g)	[b] Particle Size (nm)	[c] Bandgap (eV)	[d] Maximum Current (μA)
S1	34.7	112.9	1.33	0.18
S2	52.8	44.5	2.21	0.21
S3	76.84	25.8	2.60	0.30
S4	98.1	22.8	3.71	0.35
S5	83.52	130.9	2.68	0.33
S6	48.81	189.9	2.45	0.31

[a]BET
[b]PSA
[c]UV-DRS
[d]C-V

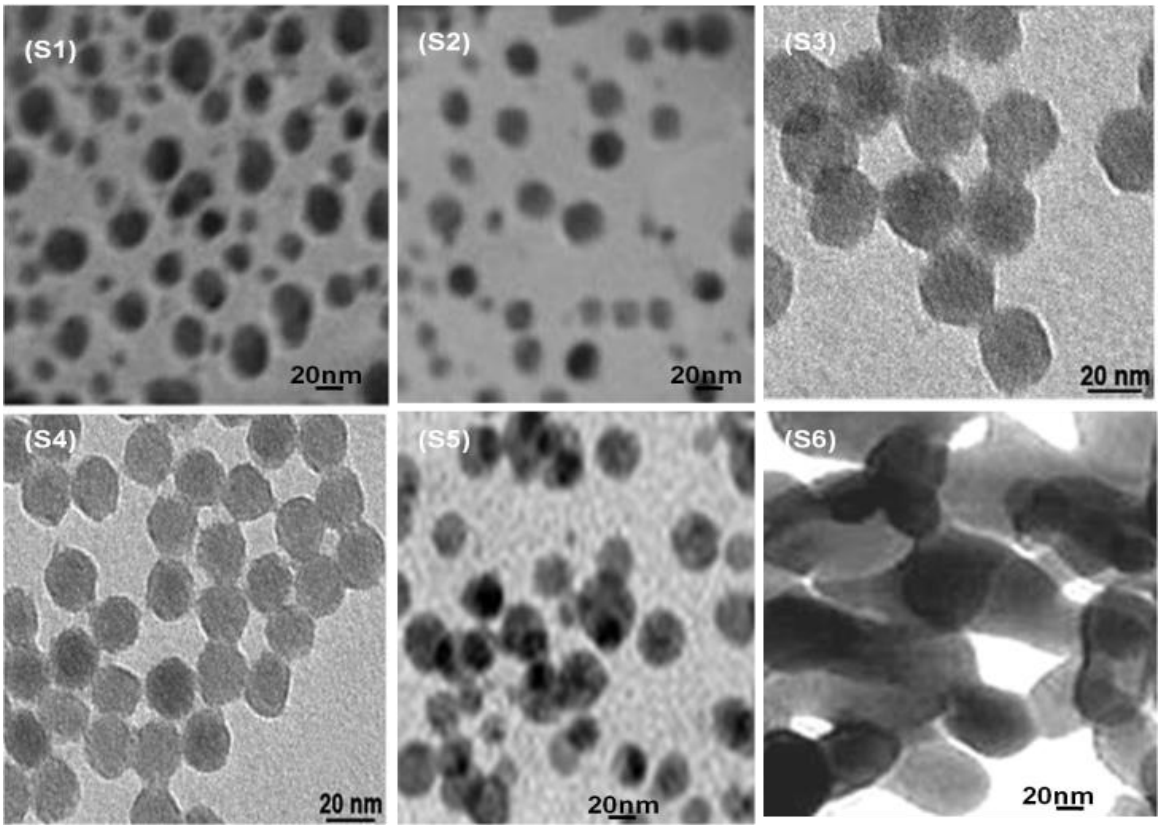

Figure 8. TEM micrographs of MoO_3 nanoparticles synthesized at (S1) 80 °C (S2) 100 °C (S3) 120 °C (S4) 150 °C (S5) 170 °C and (S6) 200 °C

Gas sensing characteristics

The gas sensing characteristics were measured for the samples S1-S6. By studying the sensor response the sample S4 exhibited high Sensitivity of S=68.5% at an operating temperature of 200 °C towards 1000 ppm CO_2 gas as shown in Figure 9**a**. The response towards different gas concentrations of CO_2 at 200 °C is depicted in Figure 9**b**. The sensing response increases with the increase in gas concentration and reaches a maximum at 1000 ppm. It is also seen that the sensor is sensitive to low concentration of 200 ppm CO_2 gas.

Response and recovery times are important parameters of gas sensors, which are defined as the time taken for the sensor to reach 90% of its total change in sensitivity after exposure to the target gas and the time taken for the sensor to reach its initial sensitivity value once the gas atmosphere ceases to exist. The MoO_3 sensor (sample S4) exhibited shorter response and recovery time of ~50 s & ~40 s respectively as shown in Figure 9**c**. The selectivity was measured for evaluating the specificity of MoO_3 sensor by comparing the effect of interfering gases. Figure 9**d** depicts the sensing response towards other interfering gases like H_2, Ethanol, Methanol, ammonia and LPG towards 1000 ppm gas at 200 °C along with CO_2 gas. The sensor had higher response to CO_2 when compared to other test gases. Therefore, according to the experimental results the sensor can selectively detect CO_2 in presence of other gases.

According to mechanical expansion property under temperature processing of a material, the material undergoes expansion till certain

temperature and loses its expanding nature above certain saturation temperature. Due to this thermal expansion property of the nano MoO_3 semiconductor material, there is a high adsorption of the gas during gas flow into the chamber which causes decrease in the resistance of the sensor material. Hence, the sensor exhibits high sensitivity at an optimum operating temperature of 200 °C. The proposed sensor is more sensitive to CO_2 compared to other gases due to the reaction between CO_2 and the chemisorbed oxygen on the nano MoO_3 surface is higher compared to other gases.

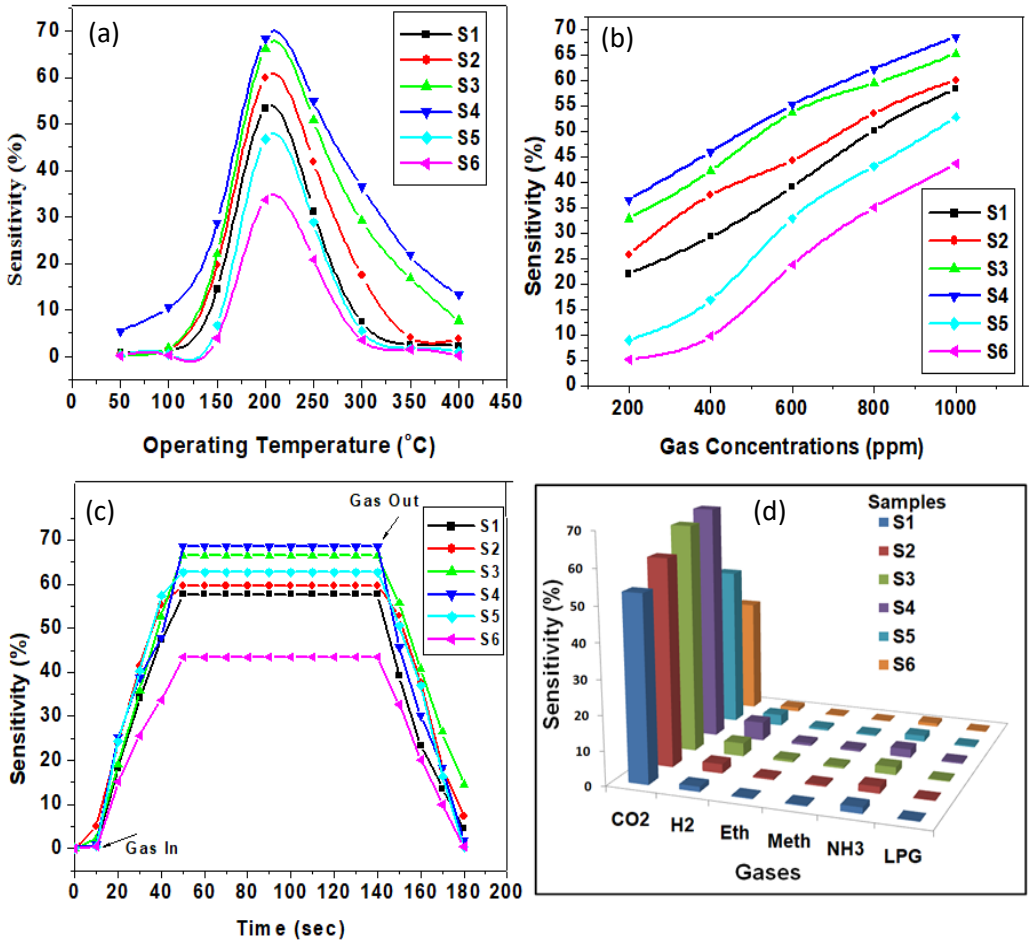

Figure 9. a) Sensor response of nano MoO_3 (S1 to S6) & Sensitivity as a function of operating temperature, b) Sensitivity Vs. gas concentrations, c) Response and Recovery Times, d) Sensitivity as a function of different gases

Gas Sensing Mechanism

The proposed gas sensing mechanism is based on the variation of the surface electron depletion region due to the reaction between CO_2 and the chemisorbed oxygen on the surface. When the semiconductor material is processed over a temperature range in air atmosphere, the oxygen molecules get adsorbed on the surface of the semiconductor and extracts electrons from the conduction band to form oxygen ions which leads to the formation of an electron depletion region near the surface due to which

there is a increase in the resistance and decrease in the net carrier density. When the sensor is exposed to CO_2, the gas molecules react with the surface oxygen species. The redox reaction is exothermic and results in fast desorption of produced CO_3^- ions from the surface. These released CO_3^- ions along with the conduction band electrons reduce the thickness of the depletion region, resulting in decrease in the resistance of the semiconductor (MoO_3) in presence of CO_2 gas and increase in sensor response (i.e., Sensitivity). When the sensor is exposed to the air ambient again, the depletion region is rebuilt by the surface oxygen species and the resistance of the semiconductor material (MoO_3) regains its initial resistance value. This is due to the accumulated layer of electrons which leads to the recovery of original resistance value [36].

$$MoO_3 + CO_2 \rightarrow MoO_2 + CO_3^{2-} \quad (3)$$

The Equation 3 depicts the release of CO_3^{2-} ions when CO_2 gas reacts with nano MoO_3 surface causing reduction in the resistance and thereby an increase in Sensitivity of the sensor.

Conclusions

In conclusion, the formation of stable MoO_3 nanoparticles with high surface area of 98.1 m^2/g and particle size of ~22 nm was obtained by optimizing the reaction condition via hydrothermal protocol. TEM micrographs confirm the orthorhombic structure of MoO_3. The optimum sensor response for S4 sample was S=68.5% towards 1000ppm CO_2 at 200 °C with response and recovery times of ~50s and ~40s respectively. The sensor exhibited excellent sensitivity and selectivity towards CO_2 gas as compared to other interfering gases The process adopted in the present study for the preparation of nano MoO_3 which is found to be novel, cost effective and suitable candidate for development of CO_2 gas sensor.

Acknowledgements

Authors gratefully acknowledge DST-IDP (GAP 0262), for financial assistance and M.V. Manasa is thankful to DST-INSPIRE Fellowship grant (GAP 0526). All Authors thank Director CSIR-IICT for support extended throughout the research work (IICT/Pubs./20212/012).

Disclosure Statement

No potential conflict of interest was reported by the authors.

Orcid

G. Sarala Devi 0000-0001-8862-3787

References

[1]. Zhenfeng B., Takashi T., Peng Z., Mamoru F., Tetsuro M. *Nature Communications*, 2014, **5**:30
[2]. Lee C.Y., Li S.Y., Lin P., Tseng T.Y. *IEEE Trans. Nanotechnol*., 2006, **5**:216
[3]. Li S.Y., Lin P., Lee C.Y., Tseng T.Y. *J. Appl. Phys*., 2004, **95**:3711
[4]. Bai S.N., Tseng T.Y., *Thin Solid Films*, 2006, **515**:872
[5]. Wang Z., Song J. *Science*, 2006, **312**:242
[6]. He H. Jr., Hsin C.L., Liu J., Chen L.J., Wang Z.L. *Adv. Mater*., 2007, **19**:781
[7]. Ra H.W., Choi K.S., Kim J.H., Hahn Y.B., Im Y.H. Small, 2008, **4**:1105
[8]. Kosta P., Giorgos A., Dimitrios A., Ahmed M., Umar D., Ioannis T., William I. M., Arokia N. and George A. *Appl. Phys. Lett.*, 2020, **116**:163505
[9]. Marabelli F., Parraviciny G.B., Drioli F.S. *Phys. Rev. B*., 1995, **52**:1433
[10]. Chen J., Deng S.Z., She J.C., Xu N.S., Zhang W.X., Wen X.G., Yang, S.H. *J. Appl. Phys*., 2003, **93**:1744
[11]. Chowdhuri A., Gupta V., Sreenivas K., Kumar R., Mozumdar S., Patanjali P.K. *Appl. Phys. Lett*., 2004, **84**:1180

[12]. Madhuri M., Subrata K., Sujit Kumar G., Sudipa P., Tapan K. S., Yusuf S.M., Tarasankar P. *J. Collo. Inter. Sci*., 2005, **286**:187
[13]. Beek B.W.J.E., Slooff L.H., Wienk M.N., Kroon J.M., Janseen R.A.J. *Adv. Funct. Mater*., 2005, **15**:1703
[14]. Sheng X., Zhong L.W. *Nano Res*., 2011, **4**:1013
[15]. Olson D.C., Piris J., Colins R.T., Shaheen S.E., Ginley D.S. *Thin Solid Films*, 2006, **496**:26
[16]. Xu Z.X., Roy V.A.L., Stallinga P., Muccini M., Toffanin S., Xiang H.F., Che C.M. *Appl. Phys. Lett*., 2007, **90**:223505
[17]. Fernandes D.M., Silva R., Winkler Hechenleitner A.A., Radovanovic E., Custódio Melo M.A., Gómez Pineda E.A., *Mater. Chem. Phy*., 2009, **115**:110
[18]. Jian F.L., Li B.L., Xue H.S., Kai D., Jing N., Chao J.L., Wei S.L. Langmuir, 2013, **29**:13975
[19]. Barsan N., Weimar U., *J. Phys. Condens. Matter*., 2003, **15**:813
[20]. Yamazoe N., Shimanoe K. *J. Sens.*, 2009, **875704**:21 pages
[21]. Sarala Devi G., Takeo H., Yasuhiro S., Makoto E. *Sensors and Actuators B*., 2002, **87**:122
[22]. Tomescu A., Simion C.E., Alexandrescu R., Morjan I., Scarisoreanu M. *Romanian J. Inf. Sci. & Tech.* 2008, **11**:85
[23]. Gajendiran J., Rajendran V. *Materials Letters*, 2014, **116**:311
[24]. Saravanana R., Karthikeyan S., Gupta V.K., Sekaran G., Narayanan V., Stephen A. *Materials Science and Engineering: C*, 2013, **33**:91
[25]. Habibi M.H., Karimi B., Zendehdel M., Habibi M. *Spectrochim Acta: A Mol Biomol Spectrosc*., 2013, **116**:374
[26]. Jianyu Y., Shendong Z., Xiaoyong X., Wenchang Z., Bing F., Jingguo H. *J. Materials Chemistry: A*, 2015, **3**:1199
[27]. Petetin L., Berger F., Chambaudet A., Planade R. *Sensors and Actuators B: Chemical*, 2001, **78**:166
[28]. Niskanen A., Varpula A., Utriainen M., Natarajan G., Cameron D. *Sensors and Actuators B: Chemical*, 2010, **148**:227.
[29]. Yadav B.C., Richa S., Dwivedi C.D., Pramanik P., *Sensors and Actuators B: Chemical*, 2008, **131**:216
[30]. Manasa M.V., Sarala Devi G., Prasada Reddy P.S., Sreedhar B. *Materials Research Express*, 2019, **6**:125041
[31]. Rosetti R., Nakahara S., Brus L.E. *Journal of Chemical Physics*, 1983, **79**:1086
[32]. Hübner M., Sinion C., Haensch A., Barsan N. and U. *Sensors and Actuators B: Chemical*, 2010 **151**:103
[33]. Ganguly A., George R. *Bulletin of Materials Science*, 2007, **30**:183
[34]. Nagabhushana G.P., Samrat D., Chandrappa G.T. *RSC Advances*, 2014, **4**:56784
[35]. Arumugam M., Gang-Juan L., Chin-Yi C., Jing-Heng C. *Materials Research Bulletin*, 2015, **62**:184
[36]. Manasa M.V., Prasada Reddy P.S., Adi Narayana Reddy B., Sarala Devi G. *Journal of Advanced Physics*, 2018, **7**:1

How to cite this manuscript:. M.V. Manasa, G. Sarala Devi*. Synthesis, structural evaluation of molybdenum oxide (MoO_3) nanoparticles and its application as CO_2 gas sensor. *Journal of Medicinal and Nanomaterials Chemistry*, 3(4) 2021, 282-294. DOI: 10.48309/JMNC.2021.4.5